$Os^{III}(N_2)Os^{II}$ Complexes at the Localized-to-Delocalized, Mixed-Valence Transition

Konstantinos D. Demadis,† El-Sayed El-Samanody, George M. Coia,‡ and Thomas J. Meyer*

Contribution from the Venable and Kenan Laboratories, Department of Chemistry, CB 3290, University of North Carolina at Chapel Hill, Chapel Hill, North Carolina 27599-3290

Received August 6, 1998

Abstract: On the basis of the appearance of ν(N≡N) from 2007 to 2029 cm^{-1} in CD_3CN, oxidation states at Os in *cis,cis*-$[(bpy)_2(Cl)Os^{III}(N_2)Os^{II}(Cl)(bpy)_2]^{3+}$ (**4**), *trans,trans*-$[(tpy)(Cl)_2Os^{III}(N_2)Os^{II}(Cl)_2(tpy)]^+$ (**5**), $[(tpm)(Cl)_2Os^{III}(N_2)Os^{II}(Cl)_2(tpm)]^+$ (**7**), and $[(Tp)(Cl)_2Os^{III}(N_2)Os^{II}(Cl)_2(Tp)]^-$ (**8**) are localized. For **5** this conclusion is reinforced by the crystal structure of the BF_4^- salt, which shows that the Os sites are unsymmetrical. Five narrow, solvent-independent bands appear in the near-infrared. They can be assigned to a combination of intervalence (IT) and interconfigurational $d\pi \rightarrow d\pi$ transitions. From integrated band intensities the magnitudes of the resonance energies from electronic coupling across the μ-N_2 bridge vary from 1500 to 2500 cm^{-1}. Intramolecular $Os^{II} \rightarrow Os^{III}$ electron transfer is rapid on the time scale for solvent reorientation, but a barrier still exists from low-frequency, coupled Os−Cl and Os−N vibrations.

Introduction

In the known mixed-valence μ-N_2 complexes of Os there is evidence for delocalized oxidation states. Examples include $[(NH_3)_5Os(N_2)Os(NH_3)_5]^{5+}$,[1] $[Cl(NH_3)_4Os(N_2)Os(NH_3)_4Cl]^{3+}$,[2] and $[(CH_3CN)(NH_3)_4Os(N_2)Os(NH_3)_4(CH_3CN)]^{5+}$.[3,4] In all three, the absence of a ν(N≡N) stretch in the infrared points to an averaged electronic environment across the μ-N_2 bridge. There is further evidence for delocalization in the X-ray crystal structure of $[(CH_3CN)(NH_3)_4Os(N_2)Os(NH_3)_4(CH_3CN)]^{5+}$ in the equivalent coordination environments at the two metal ions.

In this paper we present experimental data for a series of mixed-valence, μ-N_2 Os complexes showing that they have properties commonly associated with both localization and delocalization, but that there are localized $Os^{III}-Os^{II}$ oxidation states. They are examples at the mixed-valence, localized-to-delocalized transition.

Experimental Section

Abbreviations used in the text include the following: TBAH = tetra-*n*-butylammonium hexafluoro-phosphate {$[N(n\text{-}Bu)_4](PF_6)$}, tpy = 2,2′:6′,2″-terpyridine, bpy = 2,2′-bipyridine, tpm = tris(1-pyrazolyl)-methane, Tp^- = hydrido tris(1-pyrazolyl)borate anion, Fc^+ = ferrocenium cation, pic = 4-picoline, pz = pyrazine, IT = intervalence transfer, and MLCT = metal-to-ligand charge transfer. Ligand structures are shown in Figure 1.

The following compounds and salts appear in this study: *trans*-$[Os^{VI}(tpy)(Cl)_2(N)](PF_6)$ (**1**), $[Os^{VI}(tpm)(Cl)_2(N)](PF_6)$ (**2**), $[Os^{VI}(tpm)(Cl)_2(^{15}N)](PF_6)$ (**2***), $Os^{VI}(Tp)(Cl)_2(N)$ (**3**), $Os^{VI}(Tp)(Cl)_2(^{15}N)$ (**3***),

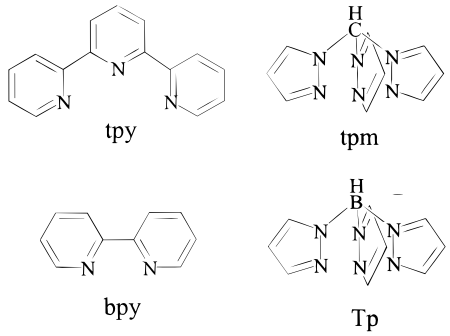

Figure 1. Ligand structures.

cis,cis-$[(bpy)_2(Cl)Os^{III}(N_2)Os^{II}(Cl)(bpy)_2](PF_6)_3$ (**4**), *trans,trans*-$[(tpy)(Cl)_2Os^{III}(N_2)Os^{II}(Cl)_2(tpy)](PF_6)$ (**5**), *trans,trans*-$[(tpy)(Cl)_2Os^{III}(^{15}N_2)Os^{II}(Cl)_2(tpy)](PF_6)$ (**5***), $(tpm)(Cl)_2Os^{II}(N_2)Os^{II}(Cl)_2(tpm)$ (**6**) $(tpm)(Cl)_2Os^{II}(^{15}N_2)Os^{II}(Cl)_2(tpm)$ (**6***), $[(tpm)(Cl)_2Os^{III}(N_2)Os^{II}(Cl)_2(tpm)](BF_4)$ (**7**), $[(tpm)(Cl)_2Os^{III}(^{15}N_2)Os^{II}(Cl)_2(tpm)](BF_4)$ (**7***), $[(Tp)(Cl)_2Os^{III}(N_2)Os^{II}(Cl)_2(Tp)](Cp_2Co)$ (**8**), $[(Tp)(Cl)_2Os^{III}(^{15}N_2)Os^{II}(Cl)_2(Tp)](Cp_2Co)$ (**8***), $[Os^{III}(tpm)(Cl)_2(NCCH_3)](PF_6)$ (**9**), and *trans*-$[Os^{III}(tpy)(Cl)_2(NCCH_3)](PF_6)$ (**10**).

Materials. CH_3CN (Burdick & Jackson) and CH_2Cl_2 (Mallinckrodt) were used as received. Deuterated solvents and isotopically labeled reagents were purchased from Cambridge Isotope Laboratories and used as received. TBAH was recrystallized three times from boiling EtOH and dried under vacuum at 120 °C for 2 days. The salts $[N(n\text{-}Bu)_4][Os(N)(Cl)_4]$,[5] *cis,cis*-$[(bpy)_2(Cl)Os^{III}(N_2)Os^{II}(Cl)(bpy)_2](PF_6)_3$ (**4**),[6,7] *trans*-$[Os^{III}(tpy)(Cl)_2(NCCH_3)](PF_6)$ (**10**),[9,10] *trans,trans*-$[(tpy)(Cl)_2Os^{III}(N_2)Os^{II}(Cl)_2(tpy)](PF_6)$ (**5**),[8,10] *trans,trans*-$[(tpy)(Cl)_2Os^{III}(^{15}N_2)Os^{II}(Cl)_2$-

† Nalco Chemical Company, Global Water Research, One Nalco Center, Naperville, IL 60563-1198.

‡ Present address: Department of Chemistry, California Institute of Technology, Pasadena, CA 91125.

(1) Richardson, D. E.; Sen, J. P.; Buhr, J. D.; Taube, H. *Inorg. Chem.* **1982**, *21*, 3136.

(2) Magnuson, R. H.; Taube, H. *J. Am. Chem. Soc.* **1972**, *94*, 7213.

(3) Che, C.-M.; Lam, H.-W.; Tong, W.-F.; Lai, T.-F.; Lau, T.-C. *J. Chem. Soc. Chem. Commun.* **1989**, 1883.

(4) Lam, H.-W.; Che, C.-M.; Wong, K.-Y. *J. Chem. Soc., Dalton Trans.* **1992**, 1411.

(5) Williams, D. S.; Coia, G. M.; Meyer, T. J. *Inorg. Chem.* **1995**, *34*, 586.

(6) Coia, G. M. Ph.D. Dissertation, The University of North Carolina, Chapel Hill, 1996.

(7) Coia, G. M.; Demadis, K. D.; Meyer, T. J. Manuscript in preparation.

(8) Demadis, K. D.; Meyer, T. J.; White, P. S. *Inorg. Chem.* **1997**, *36*, 5678.

(9) Demadis, K. D.; El-Samanody, E.-S.; Meyer, T. J.; White, P. S. *Inorg. Chem.* **1998**, *37*, 838.

(10) Demadis, K. D.; Meyer, T. J.; White, P. S. *Inorg. Chem.* **1998**, *37*, 3610.

10.1021/ja982802o CCC: $18.00
Published on Web 01/09/1999

Table 1. Summary of Crystal Data, Intensity Collection, and Structure Refinement Parameters for *trans,trans*-[(tpy)$(Cl)_2Os^{III}(N_2)Os^{II}(Cl)_2$(tpy)]$(BF_4)\cdot DMF\cdot H_2O$ (**5**)

salt	**5**	radiation	Mo Kα (λ=0.71073 Å)
formula	$Os_2Cl_4C_{33}H_{31}BF_4N_9O_2$	collection temp	−150 °C
molecular wt	1192.66	abs coeff μ, cm^{-1}	7.10
a (Å)	8.6350(1)	*F*(000)	1132.38
b (Å)	14.1004(2)	$2\theta_{max}$ (deg)	50.0
c (Å)	16.0212(1)	no. of total reflcns	16877
α (deg)	103.328(1)	no. of unique reflcns	6652
β (deg)	93.209(1)	no. of refined reflcns	4126
γ (deg)	96.412(1)	merging *R* value	0.052
V ($Å^3$)	1879.53(4)	no. of parameters	497
Z	2	*R* (%)[a]	4.8
crystal system	triclinic	R_w (%)[b]	3.9
space group	$P\bar{1}$	goodness of fit[c]	1.28
crystal size (mm)	0.03 × 0.04 × 0.15	deepest hole ($e/Å^3$)	−1.320
d_{calcd} (g/cm^3)	2.107	highest peak ($e/Å^3$)	1.430
diffractometer	siemens CCD Smart		

[a] $R = \sum(|F_o - F_c|)/\sum|F_o|$. [b] $R_w = [\sum(w|F_o - F_c|)^2/\sum w(F_o)^2]^{1/2}$ [c] GoF = $[\sum w(F_o - F_c)^2/$(no. of reflections − no. of parameters)$]^{1/2}$.

(tpy)](PF_6) (**5***),[8,10] $[Os^{III}$(tpm)$(Cl)_2(NCCH_3)](PF_6)$ (**9**),[9] and Os^{VI}(Tp)-$(Cl)_2$(N) (**3**)[11] were prepared according to literature procedures. Cobaltocene, $FcBF_4$, and NH_4PF_6 were purchased from Aldrich. KTp was purchaced from Alfa. The tpm ligand was prepared according to literature procedures.[12,13]

Physical Measurements and Instrumentation. Electronic absorption spectra were recorded on Hewlett-Packard 8452A diode array UV−vis spectrophotometers in quartz cuvettes. FT-IR spectra were recorded as KBr pellets on a Mattson Galaxy series 5000 spectrophotometer at 4 cm^{-1} resolution. Solution IR spectra were collected by using deuterated solvents and a cell with CaF_2 windows and 1.35 mm path length. Spectra in the near-IR region were recorded on a Cary model 14 spectrophotometer by using a matched pair of 2 mm path length quartz cells. Electrochemical measurements were made in CH_3CN, 0.1 M in TBAH as supporting electrolyte. A platinum disk was used for measurements as the working electrode. All potentials were referenced to the saturated sodium chloride calomel electrode (SSCE, 0.24 V vs NHE), unless otherwise noted, at room temperature and were uncorrected for junction potentials. The auxiliary electrode was a coil of platinum wire. Three compartment cells were used, with sintered glass disks separating the compartments containing reference, working, and auxiliary electrodes. Voltammetric experiments were performed with a PAR 173 galvanostat/poteniostat.

Spectral deconvolution of the near-IR bands for complexes **4**, **5**, **7**, and **8** was conducted by using a subroutine in the commercial software package GRAMS 32.

Synthesis of Compounds and Salts. [Os^{VI}(tpm)$(Cl)_2$(N)](PF_6) (2). A quantity of [N(*n*-Bu)$_4$][Os(N)$(Cl)_4$] (1.00 g, 1.69 mmol) and tpm (0.40 g, 1.86 mmol) were mixed together in CH_3OH (50 mL). The reaction mixture was stirred overnight, during which time the color turned to pink. NH_4PF_6 (1.00 g) was added as a solid to the reaction mixture. An orange solid precipitated and was filtered off, washed with EtOH, and recrystallized from CH_3CN/Et_2O and finally air-dried. Yield: 0.75 g (70%). Anal. Calcd for $C_{10}H_{10}Cl_2N_7OsPF_6$ (mol wt 634.96) C, 18.94 H, 1.59 N, 15.46. Found: C, 19.29; H, 1.73; N, 15.61. Infrared (cm^{-1}, in KBr): ν(Os≡N) 1074 (vs); ν(tpm) 1515 (vs), 1446 (vs), 1409 (vs), 1285 (vs); ν(P−F) 835 (vs).

[Os^{VI}(tpm)$(Cl)_2(^{15}N)](PF_6)$ (2*). This salt was prepared by the same method starting with $(Bu_4N)[Os(^{15}N)(Cl)_4]$. Infrared ($cm^{-1}$, in KBr): ν(Os≡^{15}N) 1053 (vs).

(tpm)$(Cl)_2Os^{II}(N_2)Os^{II}(Cl)_2(tpm)\cdot 2H_2O$ (6). A quantity of **2** (200 mg, 0.31 mmol) was dissolved in CH_2Cl_2 (200 mL). A stoichiometric amount of cobaltocene (60 mg, 0.31 mmol) was added slowly as a solid, which caused the color of the solution to turn brown. The reaction mixture was stirred at room temperature for 30 min. The solvent was taken to dryness and the resulting brown solid material was treated with 100 mL of CH_3CN to give a brown precipitate that was filtered off, washed with 3 × 30 mL of CH_3CN and Et_2O and dried. Yield: 140 mg (87%). Anal. Calcd for $C_{20}H_{20}Cl_4N_{14}Os_2\cdot 2H_2O$ (mol wt 1016.01): C, 23.67; H, 2.38; N, 19.33. Found: C, 23.79; H, 2.62; N, 17.73. Infrared (cm^{-1}, in KBr): ν(N≡N) 2040 (w); ν(tpm) 1511 (vs), 1437 (vs), 1407 (vs), 1272 (vs).

(tpm)$(Cl)_2Os^{II}(^{15}N_2)Os^{II}(Cl)_2$(tpm) (6*). This complex was prepared by the same method with $[Os^{VI}$(tpm)$(Cl)_2(^{15}N)](PF_6)$ (**2***) as the starting material. Infrared (cm^{-1}, in KBr) $\nu(^{15}N\equiv{}^{15}N)$ 1972 (w).

[(tpm)$(Cl)_2Os^{III}(N)_2Os^{II}(Cl)_2$(tpm)]$(BF_4)\cdot 2H_2O$ (7). A quantity of **6** (100 mg, 0.10 mmol) was suspended in CH_3CN (30 mL) and $FcBF_4$ (28 mg 0.10 mmol) was slowly added as a solid. The reaction mixture was stirred for 50 min. During this time the brown solid gradually disappeared and an olive green crystalline solid formed. This material was filtered off and washed with CH_3CN and Et_2O. It was then recrystallized from $DMF/CH_3CN/Et_2O$, filtered off, and air-dried. Yield: 77 mg (71%). Anal. Calcd for $C_{20}H_{20}Cl_4N_{14}Os_2BF_4\cdot 2H_2O$ (mol wt 1103.02): C, 21.81; H, 2.20; N, 17.80. Found: C, 21.72; H, 2.40; N, 16.75. Infrared (cm^{-1}, in KBr): ν(N≡N) 2029(vs); ν(tpm) 1509 (vs), 1440 (vs), 1409 (vs), 1276(vs); ν(B−F) 1062 (vs).

[(tpm)$(Cl)_2Os^{III}(^{15}N)_2Os^{II}(Cl)_2$(tpm)]$(BF_4)$ (7*) was prepared by the same method with (tpm)$(Cl)_2Os^{II}(^{15}N_2)Os^{II}(Cl)_2$(tpm) (**6***) as the starting material. Infrared (cm^{-1}, in KBr): $\nu(^{15}N\equiv{}^{15}N)$ 1965 (vs).

[(Tp)$(Cl)_2Os^{III}(N)_2Os^{II}(Cl)_2$(Tp)]$(Cp_2Co)$ (8). A quantity of **3** (60 mg, 0.12 mmol) was dissolved in CH_2Cl_2 (30 mL). Cobaltocene (11.5 mg, 0.06 mmol) was added slowly as a solid with stirring. The color turned green immediately. The reaction mixture was stirred at room temperature for 30 min. The volume of the reaction mixture was reduced to 5 mL by rotary evaporation and 400 mL of Et_2O was added to precipitate an olive green compound, which was filtered off and washed with Et_2O. This material was recrystallized from CH_3CN/Et_2O and air dried. Yield: 36 mg (50%). Anal. Calcd for $C_{28}H_{30}Cl_4N_{14}B_2Os_2Co$ (mol wt 1167.02): C, 28.86; H, 2.59; N, 16.83. Found: C, 29.43; H, 2.61; N, 14.54. Infrared (cm^{-1}, in KBr) ν(N≡N) 2011(vs); ν(Tp) 1627 (vs), 1500 (vs), 1416 (vs), 1312 (vs), 1212 (vs); ν(B−H) 2506 (vs).

[(Tp)$(Cl)_2Os^{III}(^{15}N)_2Os^{II}(Cl)_2$(Tp)]$(Cp_2Co)$ (8*). This salt was prepared by the same method starting with Os^{VI}(Tp)$(Cl)_2(^{15}N)$ as the starting material. Infrared (cm^{-1} in KBr): $\nu(^{15}N\equiv{}^{15}N)$ 1944 (vs).

X-ray Structural Determination: Data Collection, Solution, and Refinement of the Structure. Single crystals of **5** were obtained by slow diffusion of Et_2O into a 10:1 CH_3CN/DMF solution of the salt. Crystal data, intensity collection information, and structure refinement parameters for the structure are provided in Table 1. The structure was solved by direct methods. The remaining non-hydrogen atoms were located in subsequent difference Fourier maps. Empirical absorption corrections were applied with SADABS. The ORTEP plotting program was used to computer generate the structure shown in Figure 2.[14]

(11) (a) Crevier, T. J.; Mayer, J. M. *J. Am. Chem. Soc.* **1998**, *120*, 5595. (b) Crevier, T. J.; Mayer, J. M. *Angew. Chem., Int. Ed. Engl.* **1998**, *37*, 1891.

(12) Huckel, W.; Bretschneider, H. *Ber. Chem.* **1937**, *9*, 2024.

(13) Byers, P. K.; Canty, A. J.; Honeyman, R. T. *J. Organomet. Chem.* **1990**, *385*, 421.

(14) Johnson, C. K. *ORTEP: A Fortran Thermal Ellipsoid Plot Program;* Technical Report ORNL-5138; Oak Ridge National Laboratory: Oak Ridge, TN, 1976.

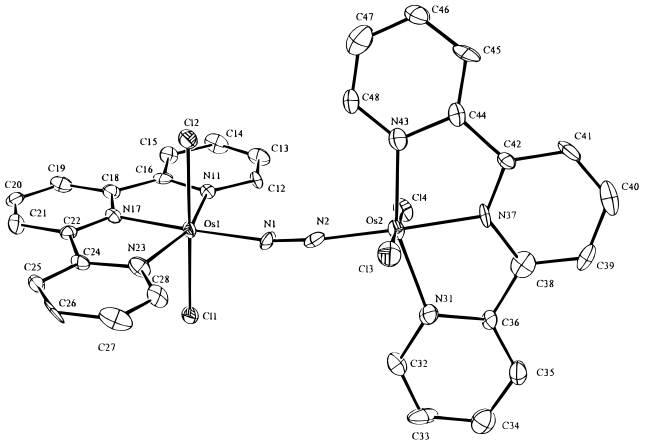

Figure 2. ORTEP diagram (30% probability ellipsoids) of the cation in *trans,trans*-$[(tpy)(Cl)_2Os^{III}(N_2)Os^{II}(Cl)_2(tpy)](BF_4)$ (**5**).

Table 2. Selected Bond Lengths (Å) and Angles (deg) for *trans,trans*-$[(tpy)(Cl)_2Os^{III}(N_2)Os^{II}(Cl)_2(tpy)](BF_4)\cdot DMF\cdot H_2O$ (5)

Bonds			
Os(l)−Cl(l)	2.352(3)	Os(2)−Cl(3)	2.401(3)
Os(l)−Cl(2)	2.371(3)	Os(2)−Cl(4)	2.402(3)
Os(l)−N(l)	1.968(9)	Os(2)−N(2)	1.909(10)
N(l)−N(2)	1.132(13)	Os(2)−N(31)	2.064(9)
Os(l)−N(11)	2.084(9)	Os(2)−N(37)	2.006(9)
Os(l)−N(17)	1.996(9)	Os(2)−N(43)	2.087(10)
Os(l)−N(23)	2.084(10)	Os(1)···Os(2)	4.9726(7)
Os(1)···B(1)	6.22	Os(2)···B(1)	6.74

Angles			
Os(l)−N(l)−N(2)	171.5(9)	Os(2)−N(2)−N(l)	172.1(9)
Cl(l)−Os(l)−Cl(2)	177.6(1)	Cl(3)−Os(2)−Cl(4)	179.0(1)
Cl(l)−Os(l)−N(l)	92.6(3)	Cl(3)−Os(2)−N(2)	91.8(3)
Cl(l)−Os(l)−N(11)	88.0(3)	Cl(3)−Os(2)−N(31)	88.3(3)
CI(l)−Os(l)−N(17)	88.9(3)	Cl(3)−Os(2)−N(37)	88.4(3)
Cl(l)−Os(l)−N(23)	91.4(3)	Cl(3)−Os(2)−N(43)	92.3(3)
Cl(2)−Os(l)−N(l)	88.6(3)	Cl(4)−Os(2)−N(2)	88.5(3)
Cl(2)−Os(l)−N(11)	89.8(3)	Cl(4)−Os(2)−N(31)	90.7(3)
Cl(2)−Os(l)−N(17)	89.8(3)	Cl(4)−Os(2)−N(37)	91.4(3)
Cl(2)−Os(l)−N(23)	90.3(3)	Cl(4)−Os(2)−N(43)	88.6(3)
N(l)−Os(l)−N(11)	97.9(4)	N(2)−Os(2)−N(31)	102.5(4)
N(l)−Os(l)−N(17)	177.5(4)	N(2)−Os(2)−N(37)	178.3(4)
N(l)−Os(l)−N(23)	102.7(4)	N(2)−Os(2)−N(43)	99.6(4)
N(11)−Os(l)−N(17)	80.2(4)	N(3l)−Os(2)−N(37)	79.2(4)
N(11)−Os(l)−N(23)	159.4(4)	N(3l)−Os(2)−N(43)	157.9(4)
N(17)−Os(l)−N(23)	79.2(4)	N(37)−Os(2)−N(43)	78.7(4)

Hydrogen atoms were included in calculated positions with thermal parameters derived from the atom to which they were bonded. All computations were performed by using the NRCVAX suite of programs.[15] Atomic scattering factors were taken from a standard source[16] and corrected for anomalous dispersion.

The crystal of **5** contains one molecule of dimethylformamide and one molecule of water per asymmetric unit. The final positional parameters, along with their standard deviations as estimates from the inverse matrix, tables of hydrogen atom parameters, anisotropic thermal parameters, and observed/calculated structure amplitudes are available as Supporting Information in a previous publication.[8] Bond lengths and angles in **5** are given in Table 2 with the numbering scheme given in Figure 2.

Results

Synthesis. Irreversible electrochemical reduction of *trans*-$[Os^{VI}(tpy)(Cl)_2(N)](PF_6)$ (**1**) occurs at $E_{p,c} = -0.36$ V vs SSCE (Table 3). Mild reducing agents, such as Et_3N, HS^-, or

(15) Gabe, E. J.; Le Page, Y.; Charland, J.-P.; Lee, F. L.; White, P. S. *J. Appl. Crystallogr.* **1989**, *22*, 384.

(16) *International Tables for X-ray Crystallography*; Kynoch Press: Birmigham, U.K., 1974; Vol. IV.

Table 3. UV−Vis, Electrochemical, and Infrared Data for Compounds and Salts **1**–**10**

complex or salt	λ_{max}, nm (ϵ, 10^3 M^{-1} cm^{-1})	solvent for cyclic voltammetry	$E_{1/2}$(**1**) (V) (III,II/II,II)	$E_{1/2}$(**2**) (V) (III,III/III,II)	other waves	IR bands (KBr, cm^{-1})
trans-$[Os^{VI}(tpy)(Cl)_2(N)](PF_6)$ **(1)**	In CH_3CN: 514 (0.13), 366 (6.7), 354 (8.5), 336 (8.7), 288 (14.8)[a]	CH_3CN			−0.36[b]	1106 ν(Os≡N)[c]
$[Os^{VI}(tpm)(Cl)_2(N)](PF_6)$ **(2)**	In CH_3CN: 446 (0.2), 270 (14.5), 250 (14.5), 212 (16.3)	CH_3CN			−0.47[b]	1076 ν(Os≡^{15}N)[c] 1074 ν(Os≡N)
$Os^{VI}(Tp)(Cl)_2(N)$ **(3)**	In CH_3CN: 454 (0.3), 240 (5.7),214 (5.9)	CH_3CN			−0.98[b]	1066 ν(Os≡N)
cis,cis-$[(bpy)_2(Cl)Os^{III}(N_2)Os^{II}(Cl)(bpy)_2](PF_6)_3$ **(4)**	In CH_3CN: ~500 (5), 378 (16), 291 (68), 248 (57)	CH_3CN	+0.56	+1.40		2011 ν(N≡N)
trans,trans-$[(tpy)(Cl)_2Os^{III}(N_2)Os^{II}(Cl)_2(tpy)](PF_6)$ **(5)**	In CH_3CN: 678 (3.8), 506 (11.2), 480 (10.2), 322 (43.3), 282 (35.1), 270 (27.9), 234 (62.8)[d]	CH_3CN	−0.05	+0.50		2007 ν(N≡N)
		CH_2Cl_2	0.00	+0.60		1942 ν(^{15}N≡^{15}N)
		DMF	−0.10	+0.46		
$(tpm)(Cl)_2Os^{II}(N_2)Os^{II}(Cl)_2(tpm)$ **(6)**	In DMSO: 476 (10.0), 436 (10.4), 386 (17.2), 360 (16.5), 280 (18.1)	DMSO	+0.04	+0.67		2040 ν(N≡N)[e] 1976 ν(^{15}N≡^{15}N)[e]
$[(tpm)(Cl)_2Os^{III}(N_2)Os^{II}(Cl)_2(tpm)](BF_4)$ **(7)**	In DMSO: 534 (0.6), 470 (1.6), 302 (16.8)	DMSO	+0.12	+0.73		2029 ν(N≡N)[e] 1965 ν(^{15}N≡^{15}N)[e]
$[(Tp)(Cl)_2Os^{III}(N_2)Os^{II}(Cl)_2(Tp)](Cp_2Co)$ **(8)**	In CH_3CN: 430 (3.0), 314 (27.4), 264 (60.3), 212 (80.9)	CH_3CN	−0.17	+0.39	−0.44[f]	2011 ν(N≡N)
$[Os^{III}(tpm)(Cl)_2(NCCH_3)](PF_6)$ **(9)**	In CH_3CN: 349 (1.6), 330 (7.3), 288 (12.3), 256 (10.6), 210 (17.9)	CH_3CN			+1.39[g] −0.09[h]	2289, 2332 ν(C≡N)
trans-$[Os^{III}(tpy)(Cl)_2(NCCH_3)](PF_6)$ **(10)**	In CH_3CN: 616 (0.4), 540 (1.2) 516 (3.5), 488 (2.5), 456 (3.2), 438 (3.1), 396 (2.4), 354 (sh, 7.9), 318 (19.4), 230 (3.6)	CH_3CN			+1.37[g] +0.04[h]	2256, 2213 ν(C≡N)

[a] Taken from: Williams, D. S.; Coia, G. M.; Meyer, T. J. *Inorg. Chem.* **1995**, *34*, 586. [b] $Os^{VI/V}$ wave. [c] Taken from: Ware, D. C.; Taube, H. *Inorg. Chem.* **1991**, *30*, 4598 (measured in a Nujol mull). [d] Taken from: Demadis, K. D.; Meyer, T. J.; White, P. S. *Inorg. Chem.* **1997**, *36*, 5678. [e] Very weak. [f] $Co(Cp)_2^{+/0}$ couple. [g] $E_{p,c}$ for the $Os^{VI/III}$ couple. [h] $Os^{III/II}$ couple.

cobaltocene, undergo rapid reactions (within seconds) with nitrido complexes **1** or **2**, to give the μ-N_2 dimers *trans,trans*-(tpy)$(Cl)_2Os^{II}(N_2)Os^{II}(Cl)_2$(tpy) and (tpm)$(Cl)_2Os^{II}(N_2)Os^{II}(Cl)_2$(tpm), respectively. They form by reduction to $Os^{V}{\equiv}N$ followed by rapid coupling to give $Os^{II}(N_2)Os^{II}$.[8,9] $E_{p,c} = -0.98$ V for the $Os^{VI/V}$ couple for **3** and cobaltocene was used as the reductant to give the mixed-valence salt [(Tp)$(Cl)_2Os^{III}(N_2)Os^{II}(Cl)_2$(Tp)]$(Cp_2Co)$ as the final product. Similar coupling reactions between Os^{VI} nitrido complexes have been reported previously by Taube[17] and Che.[3,4] Chemical oxidation of *trans,trans*-(tpy)$(Cl)_2Os^{II}(N_2)Os^{II}(Cl)_2$(tpy) or (tpm)$(Cl)_2Os^{II}(N_2)Os^{II}(Cl)_2$(tpm) with Fc^+ salts affords the mixed-valence ions *trans,trans*-[(tpy)$(Cl)_2Os^{III}(N_2)Os^{II}(Cl)_2$(tpy)]$^+$ (**5**) and [(tpm)$(Cl)_2Os^{III}(N_2)Os^{II}(Cl)_2$(tpm)]$^+$ (**7**), respectively, in good yields and ^{15}N labeled dimers **5***, **6***, **7***, and **8***, by using the corresponding ^{15}N labeled nitridos. Chemical reduction of **5** with Cu^0 affords *trans,trans*-(tpy)$(Cl)_2Os^{II}(N_2)Os^{II}(Cl)_2$(tpy) quantitatively.

The dimer *cis,cis*-[$(bpy)_2$(Cl)$Os^{III}(N_2)Os^{II}$(Cl)$(bpy)_2]^{3+}$ (**4**) was prepared by electrochemical oxidation of *cis*-[$Os^{II}(bpy)_2$(Cl)(NH_3)](PF_6) in H_2O, at pH 9.2 at a reticulated vitreous carbon electrode at $E_{app} = +0.65$ V vs SSCE. The potential was then switched to +0.30 V for reduction of the $Os^{III}-Os^{II}$ form to $Os^{II}-Os^{II}$. Addition of NH_4PF_6 caused the olive-green salt *cis,cis*-[$(bpy)_2$(Cl)$Os^{II}(N_2)Os^{II}$(Cl)$(bpy)_2$]$(PF_6)_2$ to precipitate. It was purified by cation exchange chromatography by using 0.2 M NaCl as the eluant. **4** was prepared by $(NH_4)_2$-$[Ce^{IV}(NO_3)_6]$ oxidation of the $Os^{II}-Os^{II}$ form. Details are given elsewhere.[6,7]

Molecular Structure of *trans,trans*-[(tpy)$(Cl)_2Os^{III}(N_2)Os^{II}(Cl)_2$(tpy)]$^+$ (5). Important features in this structure (Figure 2) include the nearly staggered tpy ligands with a dihedral angle of ~74° and the bent N_2 bridge with Os(1)−N(1)−N(2) and Os(2)−N(2)−N(1) angles of 171.5(9)° and 172.1(9)°, respectively. A similar bending has been observed in several homo- and heteronuclear μ-N_2 dimers based on W−Zr,[18] Zr−Zr,[19,20] Ta−Ta,[21] Fe−Mo,[22] and Nb−Nb.[23] In these cases bending is usually associated with the presence of a M−N bond order higher than 1 and N−N bond order lower than 3 implying significant electron donation to μ-N_2. In some examples the bridging N_2 unit has been formally described as hydrazido (4−), N_2^{4-}, with a N−N single bond.[21,23]

This is not the case in **5**. The N(1)−N(2) bond length is 1.132(13) Å, only slightly longer than that of free N_2 (1.0976(2) Å)[24] but much shorter than that in the complexes cited above, and similar to the N−N distance found in a plethora of other binuclear complexes.[25] The Os(1)···Os(2) distance across the bridge is 4.9726(7) Å.

The Os−N(bridge) bond lengths are slightly shorter than typical Os−N single bonds. For example, Os−N(NH_3) is 2.123(7)−2.139(6) Å in $[(CH_3CN)(NH_3)_4Os(N_2)Os(NH_3)_4(CH_3CN)]^{5+}$.[3,4] More importantly, they are not equivalent with Os(1)−N(1) = 1.968(9) Å and Os(2)−N(2) = 1.909(10) Å. There are two distinct sets of Os−Cl bond lengths: "short" bonds, Os(1)−Cl(1) = 2.352(3) Å and Os(1)−Cl(2) = 2.371(3) Å, consistent with Os^{III}−Cl,[26] and "long" bonds, Os(2)−Cl(3) = 2.401(3) Å and Os(2)−Cl(4) = 2.402(3) Å, consistent with Os^{II}−Cl.[27] The BF_4^- counterion is located 6.22 Å from Os(1) and 6.74 Å from Os(2).

On the basis of the Os−Cl bond lengths and counterion placement in the lattice there are localized Os^{III}(Os(1)) and Os^{II}(Os(2)) sites in **5** at least in the solid state. The Os^{II}(Os(2))−$N(N_2)$ bond length is shorter than Os^{III}(Os(1))−$N(N_2)$ because of Os^{II}−N back-bonding.[28]

The Os−N(tpy) bond distance to the central tpy ring is 1.996(9) Å at the Os^{III}. The other two Os−N(tpy) distances are 2.084(9) and 2.084(10) Å. The distances at Os^{II} are comparable. The shortening of the "central" M−N(tpy) bond is a characteristic of the structural chemistry of metal−terpyridine complexes (in the absence of trans influence ligands) and is shared by **5** (Table **2**).[29] It is a feature dictated by the geometrical constraints of tpy as a ligand and its inability to span the 180° required for a planar terdentate ligand. A representative example is Os^{III}(tpy)$(Cl)_3$ in which the Os−N(tpy, central) bond length is 1.969(3) Å and the remaining two bond lengths are 2.077(3) and 2.075(3) Å.[30]

UV−Vis Spectra. UV−vis absorption maxima and molar extinction coefficients are listed in Table **3**. For the μ-N_2 complexes containing polypyridyl ligands intense $d\pi(Os^{II}) \rightarrow \pi^*$(bpy) or $d\pi(Os^{II}) \rightarrow \pi^*$(tpy) metal-to-ligand charge transfer (MLCT) bands appear in the visible. The spectra of **4** and **5** and their $Os^{II}-Os^{II}$ forms are shown in Figure 3. Band energies are shifted to lower energies for **5** compared to **4**, due to the more electron rich coordination environment, consistent with $Os^{III/II}$ redox potentials (see below). Due to spin−orbit coupling,[31] the low-energy MLCT bands arise from transitions to excited state "triplets" which are actually of mixed spin character accounting for their intensities.[32]

The spectra of **6**, **7**, and **8** do not exhibit intense bands in the visible as do their polypyridyl analogues. Intense absorptions for the tpm complexes appear at higher energies which arise from a mixture of $d\pi(Os^{II}) \rightarrow \pi^*$(tpm) and $\pi \rightarrow \pi^*$ transitions. Bands in the same region have been reported for Ru^{II}−tpm complexes.[33]

(17) Ware, D. C.; Taube, H. *Inorg. Chem.* **1991**, *30*, 4605.
(18) Mizobe, Y.; Yokobayashi, Y.; Oshita, H.; Takahashi, T.; Hidai, M. *Organometallics* **1994**, *13*, 3764.
(19) Fryzuk, M. D.; Haddad, T. S.; Mylvaganam, M.; McConville, D. H.; Retting, S. J. *J. Am. Chem. Soc.* **1993**, *115*, 2782
(20) Cohen, J. D.; Mylvaganam, M.; Fryzuk, M. D.; Loehr, T. M. *J. Am. Chem. Soc.* **1994**, *116*, 9529
(21) Schrock, R. R.; Wesolek, M.; Liu, A. H.; Wallace, K. C.; Dewan, J. C. *Inorg. Chem.* **1988**, *27*, 2050.
(22) O'Donoghue, M. B.; Zanetti, N. C.; Davis, W. M.; Schrock, R. R. *J. Am. Chem. Soc.* **1997**, *119*, 2753.
(23) Dilworth, J. R.; Henderson, R. A.; Hills, A.; Hughes, D. L.; Macdonald, C.; Stephens, A. N.; Walton, D. R. M. *J. Chem. Soc., Dalton Trans.* **1990**, 1077.
(24) Wilkinson, P. G.; Houk, N. B. *J. Chem. Phys.* **1956**, *24*, 528.
(25) (a) Pelikán, R.; Boèa, R. *Coord. Chem. Rev.* **1984**, *55*, 55. (b) Henderson, R. A. *Trans. Met. Chem.* **1990**, *15*, 330. (c) Leigh, G. J. *Acc. Chem. Res.* **1992**, *25*, 177.
(26) Os^{III}−Cl bond lengths: (a) Bright, D.; Ibers, J. A. *Inorg. Chem.* **1969**, *8*, 1078. (b) Aslanov, L.; Mason, R.; Wheeler, A. G.; Whimp, P. O. *J. Chem. Soc. Chem. Commun.* **1979**, 30. (c) Champness, N. R.; Levason, W.; Mould, R. A. S.; Pletcher, D.; Webster, M. *J. Chem. Soc., Dalton Trans.* **1991**, 2777. (d) Champness, N. R.; Levason, W.; Pletcher, D.; Spicer, M. D.; Webster, M. *J. Chem. Soc., Dalton Trans.* **1992**, 2201.
(27) Os^{II}−Cl bond lengths: (a) Chakravarty, A. R.; Cotton, F. A.; Schwotzer, W. *Inorg. Chim. Acta* **1984**, *84*, 179. (b) Cotton, F. A.; Diebold, M. P.; Matusz, M. *Polyhedron* **1987**, *6*, 1131. (c) Robinson, P. D.; Ali, I. A.; Hinckley, C. C. *Acta Crystallogr.* **1991**, *C47*, 651. (d) Levason, W.; Champness, N. R.; Webster, M. *Acta Crystallogr.* **1993**, *C49*, 1884.
(28) (a) Dilworth, J. R.; Richards, R. L. In *Comprehensive Organometallic Chemistry*; Wilkinson, G., Stone, F. G. A., Abel, E. W., Eds.; Pergamon Press: Oxford, 1982; Vol. 8, p 1073, and references therein. (b) George, T. A. In *Homogeneous Catalysis with Metal Phosphine Complexes;* Pingolet, L. H., Ed.; Plenum Press: New York, 1983; p 405. (c) Chatt, J.; Dilworth, J. R.; Richards, R. L. *Chem. Rev.* **1978**, *78*, 589.
(29) (a) Beck, J.; Schweda, E.; Strähle, J. *Z. Naturforsch.* **1985**, *B40*, 1073. (b) Bardwell, D. A.; Cargill Thompson, M. W.; McCleverty, J. C.; Ward, M. D. *J. Chem. Soc., Dalton Trans.* **1996**, 873. (c) Constable, E. C. *Metals and Ligand Reactivity*; VCH Publishers: New York, 1996, and references therein.
(30) Demadis, K. D.; El-Samanody, E.-S.; Meyer, T. J.; White, P. S. Submitted for publication.
(31) Goodman, B. A.; Raynor, J. B. *Adv. Inorg. Chem. Radiochem.* **1970**, *13*, 135.

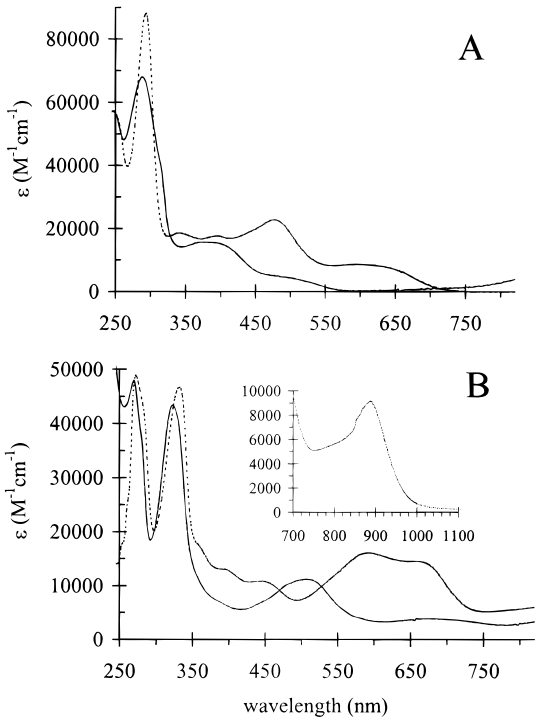

Figure 3. UV−vis spectra of *cis,cis*-$[(bpy)_2(Cl)Os^{II}(N_2)Os^{II}(Cl)(bpy)_2]^{2+}$ (- - -, in CH_3CN) and *cis,cis*-$[(bpy)_2(Cl)Os^{III}(N_2)Os^{II}(Cl)(bpy)_2]^{3+}$ (—, in CH_3CN) (A) and of *trans,trans*-$(tpy)(Cl)_2Os^{II}(N_2)Os^{II}(Cl)_2(tpy)$ (- - - and inset, in DMF) and *trans,trans*-$[(tpy)(Cl)_2Os^{III}(N_2)Os^{II}(Cl)_2(tpy)]^+$ (—, in CH_3CN) (B).

Electrochemistry. Electrochemical data are presented in Table **3**. In cyclic voltammograms of **1** in DMF, an irreversible Os^{VI}/Os^{V} wave is observed at $E_{p,c} = -0.36$ V vs SSCE. Following the reductive scan, reversible waves corresponding to the $Os^{III}-Os^{II}/Os^{II}-Os^{II}$ and $Os^{III}-Os^{III}/Os^{III}-Os^{II}$ couples of **5** appear at +0.21 and +0.77 V vs SSCE ($\Delta E_{1/2} = 560$ mV). Similar results were obtained for **2** and **3** with reduction of **2** at $E_{p,c} = -0.47$ V leading to $Os(N_2)Os$ waves at $E_{1/2} = +0.04$ and +0.67 V ($\Delta E_{1/2} = 630$ mV) and reduction at $E_{p,c} = -0.98$ V of **3** leading to waves at $E_{1/2} = -0.17$ and +0.39 V ($\Delta E_{1/2} = 560$ mV). For μ-N_2 complex **4** $E_{1/2}(1) = +0.56$, with a second wave appearing at $E_{p,a} = +1.40$ V, which is irreversible to scan rates up to 5 V/s. Exhaustive electrolysis past the irreversible wave gave $[Os^{III}(bpy)_2(Cl)(NCCH_3)]^{2+}$ based on a comparison of $E_{1/2}(Os^{III/II})$ values.[34] In CH_3CN over several hours, **5** undergoes partial solvolysis to give *trans*-$[Os^{III}(tpy)(Cl)_2(NCCH_3)](PF_6)$ (**10**) as shown by $E_{1/2}$ values for the $Os^{IV/III}$ (+1.37 V) and $Os^{III/II}$ (+0.04 V) couples (Table 3).[10] Similar observations were made for **7**. Multiple, bpy-based reductions are observed at −1.3 to −1.6 V consistent with literature values.[35]

Near-Infrared Spectra. Near-IR spectra for **4**, **5**, **7**, and **8** are shown in Figure 4 with a spectral summary in Table 4. A common pattern of five bands (labeled **I**−**V**) is observed with band **V** obscured for **5** by a low-energy $Os^{II} \rightarrow tpy$ MLCT band at 11 500 cm^{-1}. A related band is observed at 11 270 cm^{-1} in *trans,trans*-$(tpy)(Cl)_2Os^{II}(N_2)Os^{II}(Cl)_2(tpy)$ (Figure 3B, inset).[8] None of these bands are appreciably solvent dependent (Table 1 in Supporting Information). In addition, temperature-dependence studies from −38.5 to 25.0 °C in CD_3CN, from 4600 to 12600 cm^{-1}, revealed that the bands in **5** do not shift in energy, but do narrow and increase in intensity as the temperature is decreased.

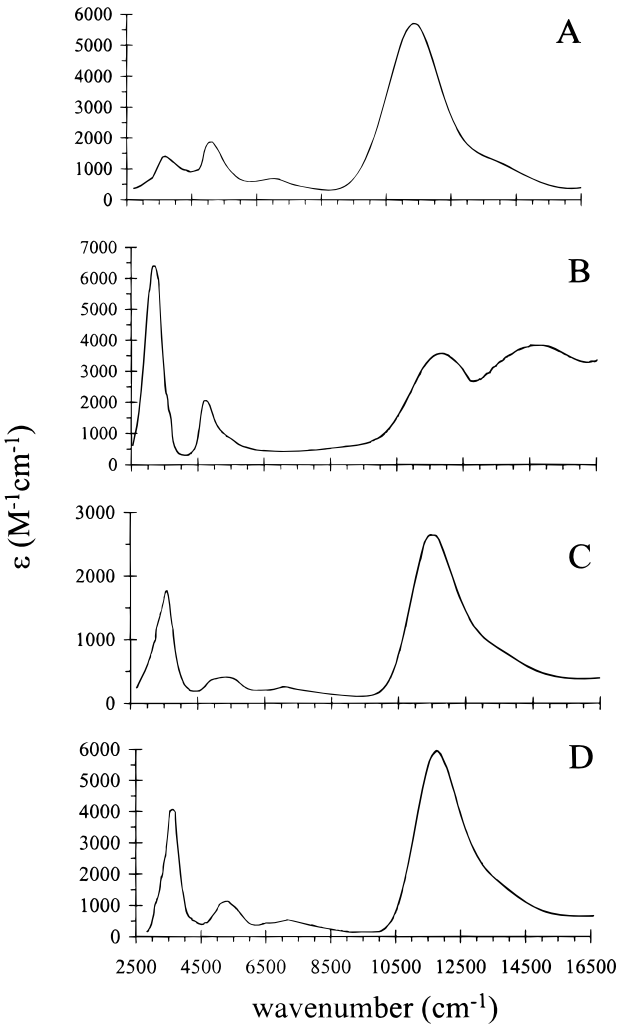

Figure 4. Near-IR spectra for *cis,cis*-$[(bpy)_2(Cl)Os^{III}(N_2)Os^{II}(Cl)(bpy)_2]^{3+}$, **4** (A, in CD_3CN), *trans,trans*-$[(tpy)(Cl)_2Os^{III}(N_2)Os^{II}(Cl)_2(tpy)]^+$, **5** (B, in CD_3CN), $[(tpm)(Cl)_2Os^{III}(N_2)Os^{II}(Cl)_2(tpm)]^+$, **7** (C, in $(CD_3)_2SO$), and $[(Tp)(Cl)_2Os^{III}(N_2)Os^{II}(Cl)_2(Tp)]^-$, **8** (D, in CD_3CN).

The spectra were scaled as $\int\epsilon(\bar{\nu})d\bar{\nu}/\bar{\nu}$ and deconvoluted by use of the software package GRAMS 32. Results of the deconvolution procedure as band maxima (E_{abs}), molar extinction coefficients (ϵ), and bandwidths ($\Delta\bar{\nu}_{1/2}$) are given in Table **4**.

In the near-IR spectra of Os^{III} complexes **9** and **10**, low-intensity bands appear at ~4100 and ~6700 cm^{-1} in CD_3CN for the expected two $d\pi \rightarrow d\pi$ interconfigurational transitions at Os^{III}.[36]

Infrared Spectra. (a) 1900−2100 cm^{-1} Region. $\nu(N\equiv N)$ appears at 2011, 2007, 2029, and 2011 cm^{-1} in KBr in μ-N_2 complexes **4**, **5**, **7**, and **8**, consistent with literature values.[37,38]

(32) (a) Richter, M. M.; Brewer, K. J. *Inorg. Chim. Acta* **1991**, *180*, 125. (b) Johnson, S. R.; Westmoreland, D. T.; Caspar, J. V.; Barqawi, K. R.; Meyer, T. J. *Inorg. Chem.* **1988**, *27*, 3195. (c) Creutz, C.; Chou, M.; Netzel, T. L.; Okamura, M.; Sutin, N. *J. Am. Chem. Soc.* **1980**, *102*, 1309. (d) Pankuch, B. J.; Lacky, D. E.; Crosby, G. A. *J. Phys. Chem.* **1980**, *84*, 2061. (e) Lacky, D. E.; Pankuch, B. J.; Crosby, G. A. *J. Phys. Chem.* **1980**, *84*, 2068. (f) Kober, E. M.; Meyer, T. J. *Inorg. Chem.* **1982**, *21*, 3967. (g) Kober, E. M.; Caspar, J. V.; Sullivan, B. P.; Meyer, T. J. *Inorg. Chem.* **1988**, *27*, 4587.

(33) (a) Llobet, A.; Hodgson, D. J.; Meyer, T. J. *Inorg. Chem.* **1990**, *29*, 3760. (b) Llobet, A.; Doppelt, P.; Meyer, T. J. *Inorg. Chem.* **1988**, *27*, 514.

(34) Kober, E. M.; Marshall, J. L.; Dressick, W. J.; Sullivan, B. P.; Caspar, J. V.; Meyer, T. J. *Inorg. Chem.* **1985**, *24*, 2755.

(35) (a) Roffia, S.; Ciano, M. *J. Electroanal. Chem.* **1979**, *100*, 809. (b) Sullivan, B. P.; Caspar, J. V.; Johnson, S. R.; Meyer, T. J. *Organometallics* **1984,** *3*, 1241. (c) Root, M. J.; Sullivan, B. P.; Meyer, T. J.; Deutsch, E. *Inorg. Chem.* **1985**, *24*, 2731.

Table 4. Spectral Parameters for Near-Infrared Bands[a]

salt	E_a, cm^{-1} (ϵ, $M^{-1}cm^{-1}$) $\Delta\bar{\nu}_{1/2}$,[c] cm^{-1} band I	band II	band III	band IV	band V
cis,cis-$[(bpy)_2(Cl)Os^{III}(N_2)Os^{II}(Cl)(bpy)_2](PF_6)_3$ (**4**)	3710 (1100) *1200*	5240 (1200) *780*	6400 (370) *2200*	11300 (5200) *1900*	13400 (900) *2400*
trans,trans-$[(tpy)(Cl)_2Os^{III}(N_2)Os^{II}(Cl)_2(tpy)](PF_6)$ (**5**)	3160 (6100) *600*	4740 (450) *600*	5200 (640) *850*	11300 (700) *1650*	11700 (1300) *1400*
$[(tpm)(Cl)_2Os^{III}(N_2)Os^{II}(Cl)_2(tpm)](BF_4)$ (**7**)	3460 (1500) *770*	5200 (230) *1100*	7000 (100) *1200*	11400 (2100) *1300*	12800 (750) *2200*
$[(Tp)(Cl)_2Os^{III}(N_2)Os^{II}(Cl)_2(Tp)](Cp_2Co)$ (**8**)	3580 (3730) *600*	5240 (930) *1100*	7070 (320) *1300*	11700 (5100) *1400*	13100 (1500) *2200*
$[Os^{III}(tpm)(Cl)_2(NCCH_3)](PF_6)$ (**9**)	4260 (180)[b] *300*	6630 (120)[b] *930*			
trans-$[Os^{III}(tpy)(Cl)_2(NCCH_3)](PF_6)$ (**10**)	4070 (65)[b] *300*	6730 (120)[b] *930*			

[a] In CD_3CN except **7** which was measured in $(CD_3)_2SO$ due to solubility limitations. By spectral deconvolution and band shape analysis. [b] $d\pi \rightarrow d\pi$ interconfigurational bands. [c] Given in italics.

These assignments are reinforced by the shifts of ~70 cm^{-1} in the ^{15}N-labeled dimers **4***, **5***, **7***, and **8*** (67 cm^{-1} calculated).

$\nu(N{\equiv}N)$ is also observed for the $Os^{II}(N_2)Os^{II}$ complexes in KBr (Table 3), but the bands are broad and intensities are lower by a factor of 10 compared to the mixed-valence complexes (e.g., $\epsilon \sim 50$ for *cis,cis*-$[(bpy)_2(Cl)Os^{II}(N_2)Os^{II}(Cl)(bpy)_2](PF_6)_2$ in CD_3CN). The origin of the intensity for $\nu(N{\equiv}N)$, which is a symmetrical stretch, is that the molecules are not totally symmetrical across the bridge. For **6**, $\nu(N{\equiv}N)$ is split in KBr with components appearing at 2088 and 2036 cm^{-1}. The origin of this splitting is presumably the existence of different rotameric forms in the KBr pellet.

(b) 1400−1500 cm^{-1} Region. ν(bpy) and ν(tpy) ring stretching vibrations appear in this region. The energies and intensities of the ν(bpy) vibrations are known to be sensitive to the Os oxidation state.[39]

For **4**, ν(bpy) bands appear at 1428, 1436, 1451, 1469, and 1496 cm^{-1} in CD_3CN. For **5**, ν(tpy) bands appear at 1436, 1449, and 1486 cm^{-1} in CD_3CN. The spectrum of **4** in this region is shown in Figure 5 and, for comparison, the sum of the spectra for *cis*-$[Os^{III}(bpy)_2(Cl)(NCCH_3)]^{2+}$ and *cis*-$[Os^{II}(bpy)_2(Cl)(NCCH_3)]^{+}$. In an earlier report, ν(bpy) modes were used as markers for localization or delocalization in $Os^{III}-Os^{II}$ mixed-valence dimers.[39]

(c) 400−600 cm^{-1} Region. Bands appear at 459, 503, and 524 cm^{-1} for *trans,trans*-$(tpy)(Cl)_2Os^{II}(N_2)Os^{II}(Cl)_2(tpy)$ and at 455, 497, and 518 cm^{-1} for *trans,trans*-$(tpy)(Cl)_2Os^{II}(^{15}N^{15}N)Os^{II}(Cl)_2(tpy)$ in KBr. Bands appear at 545, 530, and 505 cm^{-1} for $(tpm)(Cl)_2Os^{II}(N_2)Os^{II}(Cl)_2(tpm)$, and at 528, 512, and 489 cm^{-1} for $(tpm)(Cl)_2Os^{II}(^{15}N^{15}N)Os^{II}(Cl)_2(tpm)$. Following the analysis and assignments of Kettle et al.,[38] these bands can be assigned to the ν_6 (ν_{OsN_2Os}, A_{2u}), ν_{10} (δ_{OsN_2Os}, E_g), and ν_{11} (δ_{OsN_2Os}, E_u) modes of a linear (or nearly linear) Os−N−N−Os group. For $[(NH_3)_5Ru^{II}(N_2)Ru^{II}(NH_3)_5]^{4+}$, bands for these modes were assigned at 502, 520, and 316 cm^{-1}, respectively.[38]

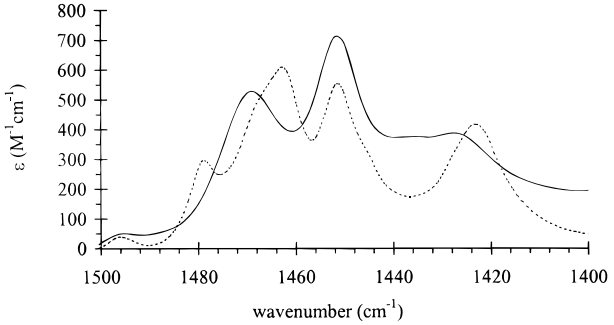

Figure 5. IR spectrum of *cis,cis*-$[(bpy)_2(Cl)Os^{III}(N_2)Os^{II}(Cl)(bpy)_2]^{3+}$ (**4**) (—) from 1400 to 1500 cm^{-1} in CD_3CN compared to the average of the sum of spectra for *cis*-$[Os^{III}(bpy)_2(Cl)(NCCH_3]^{2+}$ and *cis*-$[Os^{II}(bpy)_2(Cl)(NCCH_3)]^{+}$ (- - -).

For *trans,trans*-$(tpy)(Cl)_2Os^{II}(N_2)Os^{II}(Cl)_2(tpy)$ the relatively high band energies suggest at least partial Os−N multiple bond character. For the mixed-valence $Os^{III}(N_2)Os^{II}$ forms, there is evidence for bands in the same region, but they are of low intensity. For $[(NH_3)_5Os^{III}(N_2)Os^{II}(NH_3)_5]^{5+}$ a band in the Raman spectrum at 150 cm^{-1} has been assigned to $\nu(Os-N(N_2))$.[1]

Discussion

In a composite sense, mixed-valence complexes **4**, **5**, **7**, and **8** have some unusual properties. The major theme in this paper is to describe these properties and how they relate to electronic structure, localization vs delocalization, electronic coupling across μ-N_2, and the barrier to intramolecular electron transfer.

There is information about electronic coupling and electronic structure in the UV−visible spectra and electrochemical data. The MLCT absorption band patterns for *cis,cis*-$[(bpy)_2(Cl)Os(N_2)Os(Cl)(bpy)_2]^{3+}$ (**4**), *cis,cis*-$[(bpy)_2(Cl)Os^{II}(N_2)Os^{II}(Cl)(bpy)_2]^{2+}$, and *cis*-$[Os^{II}(bpy)_2(Cl)(NCCH_3)]^{+}$ are the same. This is illustrated in the line diagram in Scheme 1, which shows the systematic energy increases through the series. The shifts are of the same magnitude as the differences in $E_{1/2}(Os^{III/II})$, Table 3, consistent with the MLCT character of the transitions.[32f,g]

The common $d\pi \rightarrow \pi^*$(bpy) MLCT band pattern suggests that there is no major perturbation in the $d\pi$ orbitals due to electronic coupling across μ-N_2. The energy shifts are a measure of the increase in $d\pi-\pi^*$ back-bonding at $[(bpy)_2(Cl)Os^{II}]$- as the sixth ligand is varied in the series: CH_3CN, $[(N_2)Os^{II}(Cl)(bpy)_2]^{+}$, and $[(N_2)Os^{III}(Cl)(bpy)_2]^{2+}$. This also explains the decrease in band energy of $\nu(N{\equiv}N)$ in $[(bpy)_2(Cl)Os^{III}(N_2)$-

(36) (a) Sen, J.; Taube, H. *Acta Chem. Scand.* **1979**, *A33*, 125. (b) Taube, H. *J. Pure. Appl. Chem.* **1979**, *51*, 901. (c) Creutz, C.; Chou, M. H. *Inorg. Chem.* **1987**, *26*, 2995. (d) Dubicki, L.; Ferguson, J.; Krautz, E. R.; Lay, P. A.; Maeder, M.; Taube, H. *J. Phys. Chem.* **1984**, *88*, 3940. (e) Aràneo, A.; Mercati, G.; Morazzoni, F.; Napoletano, T. *Inorg. Chem.* **1977**, *16*, 1196.

(37) (a) Henderson, R. A.; Leigh, G. J.; Pickett, C. J. *Adv. Inorg. Chem. Radiochem.* **1983**, *27*, 197. (b) Hidai, M.; Mizobe, Y. *Chem. Rev.* **1995**, *95*, 1115. (c) Bee, M. W.; Kettle, S. F. A.; Powell, D. B. *Spectrochim. Acta* **1974**, *30A*, 1637.

(38) Bee, M. W.; Kettle, S. F. A.; Powell, D. B. *Spectrochim. Acta* **1975**, *31A*, 89.

(39) (a) Demadis, K. D.; Neyhart, G. A.; Kober, E. M.; Meyer, T. J. *J. Am. Chem. Soc.* **1998**, *120*, 7121. (b) Demadis, K. D.; Neyhart, G. A.; Kober, E. M.; Meyer, T. J.; White, P. S. Manuscript in preparation.

Scheme 1

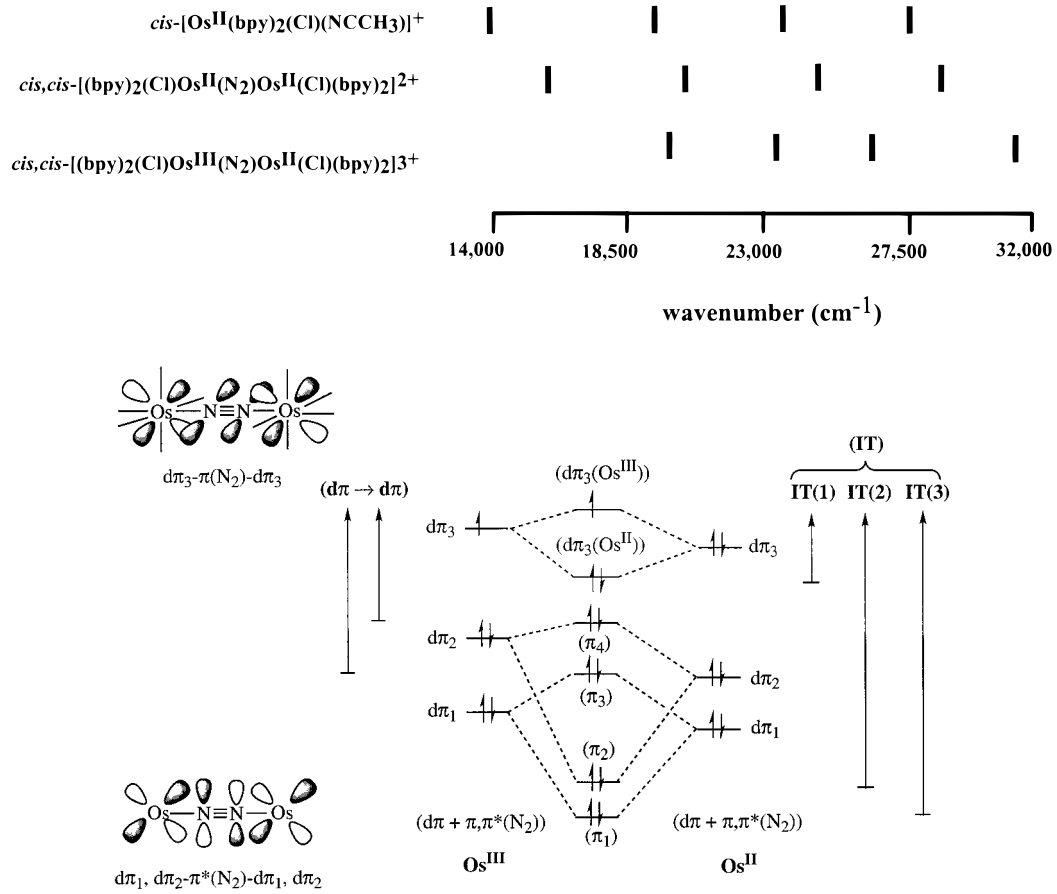

Figure 6. Schematic energy level diagram for $Os^{III}(N_2)Os^{II}$. The relative energy levels shown are those for $[(tpm)(Cl)_2Os^{III}(N_2)Os^{II}(Cl)_2(tpm)]^+$ (**7**).

$Os^{II}(Cl)(bpy)_2]^{3+}$ (**4**), compared to *cis,cis*-$[(bpy)_2(Cl)Os^{II}(N_2)$-$Os^{II}(Cl)(bpy)_2]^{2+}$. Similar arguments can be made in comparing the MLCT spectra of *trans,trans*-$(tpy)(Cl)_2Os^{II}(N_2)$-$Os^{II}(Cl)_2(tpy)$ and **5**.

Another measure of interactions across the μ-N_2 bridge is $\Delta E_{1/2}$ ($=E_{1/2}(2) - E_{1/2}(1)$) for the $Os^{III}-Os^{III}/Os^{III}-Os^{II}$ and $Os^{II}/Os^{II}-Os^{II}$ couples. $\Delta E_{1/2}$ for dimers **5**, **7**, and **8** fall in the range 0.55−0.61 V; for **4**, $\Delta E_{1/2}$ is 0.84 V. For comparison, $\Delta E_{1/2}$ is 1.20 V for $[(NH_3)_5Os(N_2)Os(NH_3)_5]^{5+}$ [1] and 0.47 V for $[(NH_3)_5$-$Ru(N_2)Ru(NH_3)_5]^{4+}$.[1] $\Delta E_{1/2}$ is related to $\Delta G°$ for the comproportionation equilibrium,

$$Os^{III}-Os^{III} + Os^{II}-Os^{II} \rightarrow 2Os^{III}-Os^{II} \qquad (1)$$

by $\Delta G°_{com}$ (in eV) $= -\Delta E_{1/2}$.

Description of Electronic Structure in the Mixed-Valence Complexes. For the mixed-valence μ-N_2 complexes $[(CH_3$-$CN)(NH_3)_4Os^{III}(N_2)Os^{II}(NH_3)_4(CH_3CN)]^{5+}$ [3,4] and $[(NH_3)_5Os^{III}$-$(N_2)Os^{II}(NH_3)_5]^{5+}$ [1] ν(N≡N) is not observed or is of low intensity. This is consistent with delocalization and no permanent dipole across μ-N_2 on the IR time scale. By contrast, relatively intense ν(N≡N) bands appear for **4**, **5**, **7**, and **8** ($\epsilon \sim 300$ for **4** and 1220 for **5**, $\epsilon = 320$ for **7** and 400 for **8**). The appearance of ν(N≡N) provides evidence for a permanent dipole moment and an oxidation state marker for $Os^{III}(N_2)Os^{II}$ on the infrared time scale. Based on the bandwidth at half-height and the uncertainty relation, $\Delta E \cdot \Delta t \leq \hbar$, it is possible to set a lower limit on the time scale for intramolecular electron transfer. For **5** with $\bar{\nu}_{1/2} = 40$ cm^{-1}, $\Delta t \leq 1 \times 10^{-13}$ s.

There is also evidence for localization in the crystal structure of **5** including short and long Os−N(bridge) bonds, short and long Os−Cl bonds, and the asymmetrical disposition of the BF_4^- counterion in the lattice. As shown by the appearance of ν(N≡N) in both CD_3CN and KBr, *localization is not simply a solid-state effect*.

Assuming localization, it is possible to assign the near-IR bands by using the schematic orbital diagram in Figure 6. In constructing the diagram, it was assumed that $d\pi(Os^{III})$ and $d\pi$-(Os^{II}) are premixed with $\pi(N_2)$ and $\pi^*(N_2)$. These orbitals promote $d\pi(Os^{III})-\pi(N_2)-d\pi(Os^{II})$ and $d\pi(Os^{III})-\pi^*(N_2)-d\pi$-$(Os^{II})$ coupling across the bridge. Taking $Os-N_2-Os$ as the *z*-axis (neglecting the slight divergence from 180°), $d\pi_1(Os^{II})$ and $d\pi_2(Os^{II})$ are largely d_{xz}, d_{yz} in character and $d\pi_3(Os^{II})$ is largely d_{xy}. Spin−orbit coupling at Os^{III} imparts *z* character to all three $d\pi(Os^{III})$ orbitals.[40,41] In Figure 6, it is assumed that $d\pi_1$ and $d\pi_2$ are strongly mixed with $\pi^*(N_2)$ orbitals to give the series of molecular orbitals π_1, π_2, π_3, and π_4. The overlaps are illustrated in Figure 6. The $d\pi_3$ orbitals are less strongly coupled. As illustrated by the overlaps in Figure 6, they have δ symmetry along the Os−N−N−Os axis and coupling across the ∼5 Å Os···Os separation distance occurs by mixing with $\pi(N_2)$.

In Figure 6 it is assumed that $d\pi_3-\pi(N_2)-d\pi_3$ mixing is relatively weak, resulting in electronically coupled but discrete $d\pi_3(Os^{III})$ and $d\pi_3(Os^{II})$ levels. The $d\pi_3-\pi(N_2)-d\pi_3$ mixing destabilizes $d\pi_3(Os^{III})$ and $d\pi_1$,$d\pi_2-\pi^*(N_2)$ mixing stabilizes $d\pi_1$ and $d\pi_2$ at Os^{II} relative to $d\pi_3$. The latter is the origin of

(40) Kober, E. M. Ph.D. Dissertation, The University of North Carolina, Chapel Hill, 1982.
(41) Kober, E. M.; Meyer, T. J. *Inorg. Chem.* **1983**, *22*, 1614.

the back-bonding effect that causes the decrease in ν(N≡N) in $Os^{III}-Os^{II}$ compared to $Os^{II}-Os^{II}$.

On the basis of this model, three IT bands and two $d\pi \rightarrow d\pi$ interconfigurational bands at Os^{III} are predicted. The latter are expected to appear in the near-IR[8,36,39−42] and, in the tentative band assignments in Figure 6, are assigned as the two transitions at lowest energy. They appear at ∼4200 and ∼6700 cm^{-1} in the $Os^{III}-NCCH_3$ complexes (**9** and **10**).

In *cis*-$[(bpy)_2(Cl)Os^{III}(pz)Ru^{II}(NH_3)_5]^{4+}$ electronic coupling causes the $d\pi-d\pi$ bands to shift to lower energy and gain intensity by mixing with the IT transitions.[39,42] The orbital basis for the mixing is $d\pi-d\pi$ coupling across the pz bridge.

On the basis of this precedence, we assign the bands at 3160−3710 cm^{-1} and 4740−5240 cm^{-1} for **4**, **5**, **7**, and **8** to $d\pi \rightarrow d\pi$ transitions, although it must be admitted that these assignments are somewhat speculative. With this assignment, the decrease in energy and higher absorptivity compared to the $Os^{III}-NCCH_3$ complexes in Table 4, is a consequence of electronic coupling across the bridge. More importantly, the energies of the proposed IT and $d\pi \rightarrow d\pi$ bands are internally consistent, at least for **4**, **7**, and **8**, see below.

Taking $[(tpm)(Cl)_2Os^{III}(N_2)Os^{II}(Cl)_2(tpm)]^+$ (**7**) as the example, the near-IR bands can be assigned according to Figure 6 as follows: (1) The two lowest energy bands are $d\pi \rightarrow d\pi$ transitions decreased in energy and enhanced in intensity by orbital mixing across the bridge which imparts some IT character. (2) The lowest energy IT band, IT(1), appears at ∼7000 cm^{-1}, see Table 4. It arises from the transition $d\pi_3(Os^{II}) \rightarrow d\pi_3(Os^{III})$. Its absorptivity is low because electronic coupling is by a δ interaction and $d\pi_3-\pi(N_2)-d\pi_3$ mixing across the N_2 bridge. A closely related orbital scheme has been proposed for $[(bpy)_2(Cl)Os^{III}(pz)Ru^{II}(NH_3)_5]^{4+}$.[42] In this case the δ interaction is sufficiently weak that IT(1) is not observed, in part due to the longer M−M distance for pyrazine as a bridge (6.9 Å) compared to N_2 (5.0 Å).[42] (3) IT(2) and IT(3) appear at 11 400 and 12 800 cm^{-1}. They are at higher energy because they involve charge transfer from $d\pi_1(Os^{II})$ and $d\pi_2(Os^{II})$, which are inner orbitals. These transitions give interconfigurational excited states, e.g., $d\pi_1^2d\pi_2^2d\pi_3^2(Os^{II})-d\pi_3^1(Os^{III}) \rightarrow d\pi_1^1d\pi_2^1d\pi_3^2(Os^{III})-d\pi_3^2(Os^{II})$.

Based on Figure 6, the energies of the IT and $d\pi \rightarrow d\pi$ bands are related as $E_{IT}(2) \approx E_{IT}(1) + E_{d\pi\rightarrow d\pi}(1)$, $E_{IT}(3) \approx E_{IT}(1) + E_{d\pi\rightarrow d\pi}(2)$. For IT(2) and IT(3) the experimental values, 11 400 and 12 800 cm^{-1}, are close to the calculated values of 10 420 and 12 160 cm^{-1}. For IT(2), the absorptivity is greatly enhanced compared to IT(1) because of extensive $d\pi_1,d\pi_2(Os^{II})-\pi^*(N_2)$ mixing across the bridge. This mixing may greatly decrease the extent of charge transfer for IT(2) compared with IT(1).

Although the proposed assignments are internally consistent, the absence of a solvent dependence for the IT bands must still be explained. Because of their charge-transfer character, they are predicted to be solvent dependent.[43] This is the case for *cis,cis*-$[(bpy)_2(Cl)Ru^{III}(pz)Ru^{II}(Cl)(bpy)_2]^{3+}$, for example, for which $Ru^{II} \rightarrow Ru^{III}$ IT bands appear in the near infrared which are broad ($\Delta\bar{\nu}_{1/2}$ = 4900 cm^{-1} in CD_3CN) and vary with the solvent dielectric function, $1/D_{op} - 1/D_s$.[44] D_{op} and D_s are the optical and static dielectric constants of the solvent. By contrast, in a range of solvents including CD_3NO_2 (D_{op} = 1.909) and $(CD_3)_2SO$ (D_{op} = 2.182), the near-IR band energies and shapes for **5** are relatively unchanged (Supporting Information, Table 1).

A related observation has been made for IT(2) and IT(3) in *cis*-$[(bpy)_2(Cl)Os^{III}(pz)Ru^{II}(NH_3)_5]^{4+}$. These are cross-bridge transitions and the absence of a solvent dependence was explained by invoking extensive $d\pi(Os^{III})-\pi,\pi^*(pz)-d\pi(Ru^{II})$ mixing, which greatly decreases the extent of charge transfer.[45] IT(1) was not observed for this complex.

There may be another explanation for **4**, **5**, **7**, and **8** based on time scale. IT(1) is expected to have charge-transfer character since $d\pi-\pi(N_2)-d\pi$ coupling is moderate at best (vide infra). If the time scale for intramolecular $Os^{III} \leftrightarrow Os^{II}$ electron transfer is rapid on the time scale for the solvent motions coupled to electron transfer, the solvent polarization surrounding the ion will assume an average of those for $Os^{III}-Os^{II}$ and $Os^{II}-Os^{III}$. The solvent would no longer contribute to the optical or thermal barriers to electron transfer.

There are two contributions to λ_o, one from dipole reorientation, λ_{oo}, and one from collective translations, λ_{oi}, analogous to phonons in the solid state. The former dominates in polar solvents.[43,46] From frequency-dependent dielectric and ultrafast transient absorption measurements in polar organic solvents, the time scales of the two motions are of the order ∼1 ps and <0.1 ps, respectively.[47]

For Gaussian absorption bands it is possible to calculate the electronic resonance energy arising from $d\pi-\pi,\pi^*(N_2)-d\pi$ mixing by using an equation derived by Hush,[48]

$$H_{DA} = \left(\frac{4.2 \times 10^{-4}\, \epsilon_{max} \Delta\bar{\nu}_{1/2} E_{abs}}{d^2}\right)^{1/2} \qquad (2)$$

In this equation, ϵ_{max} is the molar extinction coefficient (in M^{-1} cm^{-1}) at the absorption maximum, E_{abs} (in cm^{-1}), for the spectrum scaled as $\int\epsilon(\bar{\nu})\, d\bar{\nu}/\bar{\nu}$.[48,49] $\Delta\bar{\nu}_{1/2}$ is the bandwidth at half-height (in cm^{-1}). d is the metal−metal separation distance (in Å).

The spectra in Figure 4 are replotted as $\int\epsilon(\bar{\nu})\, d\bar{\nu}/\bar{\nu}$ in Figure 1 in the Supporting Information. A spectral deconvolution procedure was used to isolate the individual absorption bands and calculate ϵ_{max}, E_{abs}, and $\bar{\nu}_{1/2}$ for each component (see Experimental Section). The band-shape parameters are given in Table 4. H_{DA} values for each IT band were calculated by using eq 2, and total resonance energies from the sum are also listed in Table 5. In these calculations d was taken as 5.0 Å from the crystal structure of **5**. This is an upper limit because, as noted by Hupp, electronic coupling across the bridge

(42) Neyhart, G. A.; Timpson, C. J.; Bates, W. D.; Meyer, T. J. *J. Am. Chem. Soc.* **1996**, *118*, 3730.

(43) Chen, P.; Meyer, T. J. *Chem. Rev.* **1998**, *98*, 1439.

(44) (a) Callahan, R. W.; Meyer, T. J. *Chem. Phys. Lett.* **1976**, *39*, 82. (b) Callahan, R. W.; Keene, F. R.; Meyer, T. J.; Salmon, D. J. *J. Am. Chem. Soc.* **1977**, *99*, 1064.

(45) (a) Gress, M. E.; Creutz, C.; Quicksall, C. O. *Inorg. Chem.* **1981**, *20*, 1522. (b) Creutz, C.; Chou, M. H. *Inorg. Chem.* **1981**, *20*, 1522. (c) Wishart, J. F.; Bino, A.; Taube, H. *Inorg. Chem.* **1986**, *25*, 3318.

(46) (a) Marcus, R. A. In *Tunneling in Biological Systems*; Chance, B., DeVault, D. C., Frauenfelder, H., Marcus, R. A., Schrieffer, J. R., Sutin, N., Eds.; Academic Press: New York, 1979; p 109. (b) Marcus, R. A. *J. Chem. Phys.* **1956**, *24*, 979. (c) Marcus, R. A. *J. Chem. Phys.* **1956**, *24*, 966.

(47) (a) Dogonadze, R. R.; Kalman, E.; Kornyshev, A. A.; Ulstrup, J., Eds. *The Chemical Physics of Solvation, Part. A*; Elsevier Science Publishers B.V.: Amsterdam, 1985. (b) Ulstrup, J. *Charge-Transfer processes in Condensed Media. Lecture Notes in Chemistry;* Springer-Verlag: New York, 1979; Vol. 10. (c) Böttcher, C. J. F. *Theory of Electric Polarization*; Elsevier Publishing Co.: New York, 1952. (d) Fröhlich, H. *Theory of Dielectrics;* Oxford University Press: Oxford, 1949. (e) Cole, R. H. In *Molecular Liquids-Dynamics and Interactions;* Barnes, A. J., *et al.*, Eds.; D. Reidel Publishing Co.: New York, 1984; p 59.

(48) (a) Hush, N. S. *Prog. Inorg. Chem.* **1967**, *8*, 391. (b) Hush, N. S. *Electrochim. Acta* **1968**, *13*, 1005. (c) Creutz, C. *Prog. Inorg. Chem.* **1983**, *30*, 1.

(49) Reimers, J. R.; Hush, N. S. *Inorg. Chem.* **1990**, *29*, 3686.

Table 5. Calculated Values for H_{DA} in cm^{-1} for 4, 5, 7, and 8. The Labels 1, 2, and 3 Correspond to Bands III, IV, and V in Table 4

complex	H_{DA} (1), cm^{-1}	H_{DA} (2), cm^{-1}	H_{DA} (3), cm^{-1}	H_{DA}(total), cm^{-1}	solvent
cis,cis-$[(bpy)_2(Cl)Os^{III}(N_2)Os^{II}(Cl)(bpy)_2]^{3+}$ **(4)**	295	1369	697	2361	CD_3CN
trans,trans-$[(tpy)(Cl)_2Os^{III}(N_2)Os^{II}(Cl)_2(tpy)]^+$ **(5)**	218	468	598	1284	CD_3CN
$[(tpm)(Cl)_2Os^{III}(N_2)Os^{II}(Cl)_2(tpm)]^+$ **(7)**	118	723	595	1436	$(CD_3)_2SO$[a]
$[(Tp)(Cl)_2Os^{III}(N_2)Os^{II}(Cl)_2(Tp)]^-$ **(8)**	222	1184	852	2271	CD_3CN

[a] $(CD_3)_2SO$ was used as the solvent due to the poor solubility of its salts in CD_3CN.

decreases the actual charge-transfer distance from the geometrical distance.[50] H_{DA}(total) values are in the range 1500−2500 cm^{-1} with the most important contribution from $H_{DA}(2)$. On the basis of this analysis, the resonance energy arising from $d\pi_3(Os^{III})-d\pi_3(Os^{II})$ coupling, $H_{DA}(1)$, is relatively low, consistent with the proposed, largely $\delta-\delta$ nature of the interaction and small $d\pi-\pi(N_2)-d\pi$ mixing.

The magnitudes of the H_{DA} values reveal that through-bridge electronic coupling is moderate, at best, smaller than typical reorganizational energies and insufficient to cause a major electronic perturbation. This is consistent with the conclusions reached in interpreting the UV−visible spectra of **4** and **5**. On the basis of the total H_{DA} values, the contribution of electronic delocalization in the mixed-valence ions to ΔG°_{com} for the equilibrium in eq 1 is $2H_{AD} = 0.58$ eV (out of 0.84 eV) for **4**, 0.32 eV (out of 0.55 eV) for **5**, 0.36 eV (out of 0.61 eV) for **7**, and 0.56 eV (out of 0.56 eV) for **8**. Electronic delocalization in the mixed-valence ion accounts for >50% of the magnitude of ΔG°_{com} in these mixed-valence equilibria.

Intramolecular Electron Transfer. With the assumption of localized oxidation states, intramolecular electron transfer occurs between Os^{II} and Os^{III} across the μ-N_2 bridge with a characteristic rate constant, k_{ET}, and lifetime τ_{ET} ($=k_{ET}^{-1}$). This is illustrated for the tpm dimer, **7**, in eq 3.

$$[(tpm)(Cl)_2Os^{III}(N_2)Os^{II}(Cl)_2(tpm)]^+ \underset{k_{-ET}}{\overset{k_{ET}}{\rightleftharpoons}} [(tpm)(Cl)_2Os^{II}(N_2)Os^{III}(Cl)_2(tpm)]^+ \quad (3)$$

The various spectroscopic markers provide estimates for τ_{ET}. From the 40 cm^{-1} bandwidth at half-height for **4**, $\tau_{ET} \leq 0.1$ ps. From the absence of a significant solvent dependence for the IT bands, $\tau_{ET} < 1$ ps.

There is a third marker relating time scale and electron transfer. It is based on the series of ν(bpy) ring stretching modes in the mid-IR from 1400 to 1500 cm^{-1} shown in Figure 5.[51] In *cis,cis*-$[(bpy)_2(Cl)Os(BL)Os(Cl)(bpy)_2]^{3+}$ there are separate sets of ν(bpy) bands for Os^{II} and Os^{III} for BL = 4,4′-bpy, but for BL = pz, they are averaged.[39] The same comparisons cannot be made for **4** because of the instability of the $Os^{III}-Os^{III}$ form toward loss of N_2. Nonetheless, by comparing the data with the average of the sum of spectra for *cis*-$[Os^{III}(bpy)_2(Cl)(NCCH_3)]^{2+}$ and *cis*-$[Os^{II}(bpy)_2(Cl)(NCCH_3)]^+$ as in Figure 5, it is clear that the band positions in the mixed-valence ion *are not simply the sum* of the bands for Os^{III} and Os^{II}.

Although the solvent and ν(bpy) marker vibrations may be averaged, there is a residual barrier to intramolecular electron transfer. There is information about the barrier in the X-ray crystal structure and the differences in Os−N and Os−Cl bond distances, which implicates low-frequency Os−N and Os−Cl vibrations as contributors to the barrier.

The low-energy orbital pathway for intramolecular electron transfer is $d\pi_3(Os^{II}) \rightarrow d\pi_3(Os^{III})$. The optical analogue in the near-IR spectra is IT(1). In the classical limit, k_{ET} is given by,

$$k_{ET} = \nu_{ET} \exp(-\Delta G^*/RT) \quad (4)$$

In eq 4 ν_{ET} is the frequency factor for electron transfer and ΔG^* the free energy of activation. λ is the reorganizational energy and includes the sum of λ's for the coupled low-frequency metal−ligand vibrations and $\lambda_{o,i}$ is the translational component of λ_o,

$$\lambda = \lambda_{o,i} + \sum_l S_l \hbar\omega_l \quad (5)$$

In eq 5 the S_l and ω_l are electron-vibrational coupling constants and quantum spacings and the sum is over the coupled vibrations, l. ΔG^* is related to λ and $H_{DA}(1)$ as shown in eq 6.[48,52]

$$\Delta G^* = \frac{\lambda}{4} - H_{DA}(1) + \frac{[H_{DA}(1)]^2}{\lambda} \quad (6)$$

The magnitude of $H_{DA}(1)$ is sufficient that electron transfer occurs in the adiabatic regime and ν_{ET} is dictated by the dynamics of the coupled vibrations.[53] By using $\nu_{ET} = 10^{13}$ s^{-1}, eqs 4 and 6, the E_{abs} values in Table 4 and $H_{DA}(1)$ in Table 5, $k_{ET}(CH_3CN, 298\ K) = 1.7 \times 10^{10}$ (**4**), 5.2×10^{10} (**5**), 3.8×10^9 (**7**, in DMSO), and 5.6×10^9 (**8**) s^{-1}. These values approach but are too slow to be consistent with the time scale markers.[54]

This discrepancy can be explained by invoking an important contribution from quantum vibrational transitions below the barrier crossing (nuclear tunneling). The differences in Os−Cl and Os−$N(N_2)$ bond distances in the structure of *trans,trans*-$[(tpy)(Cl)_2Os^{III}(N_2)Os^{II}(Cl)_2(tpy)](PF_6)$ (**5**) in Table 2 are small compared to equivalent changes in isolated Os^{III} and Os^{II} complexes: $\Delta r(Os-Cl) = r(Os^{II}-Cl) - r(Os^{III}-Cl) = 0.042$ Å in **5** compared to $\Delta r(Os-Cl) = 0.080$ Å in *cis*-$[Os^{II}(bpy)_2(Cl)(NCCH_3)]^+$ and *cis*-$[Os^{III}(bpy)_2(Cl)(NCCH_3)]^{2+}$.[55] The small bond distance changes are a consequence of electronic coupling

(50) Hupp, J. T.; Dong, Y.; Blackburn, R. L.; Lu, H. *J. Phys. Chem.* **1993**, *97*, 3278.

(51) (a) Omberg, K. M.; Schoonover, J. R.; Treadway, J. A.; Leasure, R. M.; Dyer, R. B.; Meyer, T. J. *J. Am. Chem. Soc.* **1997**, *119*, 7013. (b) Mallick, P. K.; Danzer, G. D.; Strommen, D. P.; Kincaid, J. R. *J. Phys. Chem.* **1988**, *92*, 5628. (c) Strommen, D. P.; Mallick, P. K.; Danzer, G. D.; Lumpkin, R. S.; Kincaid, J. R. *J. Phys. Chem.* **1990**, *94*, 1357.

(52) (a) Hush, N. S. In *Mixed-Valence Compounds*; Brown, D. B., Ed.; Reidel Publishing Company: Dordrecht, 1980; p 151. (b) Cribb, P. H.; Nordholm, S.; Hush, N. S. in *Tunneling in Biological Systems*; Chance, B., DeVault, D. C., Frauenfelder, H., Marcus, R. A., Schrieffer, J. R., Sutin, N., Eds.; Academic Press: New York, 1979; p 139.

(53) (a) Marcus, R. A. *Annu. Rev. Phys. Chem.* **1966**, *15*, 155. (b) Marcus, R. A.; Sutin, N. *Biophys. Biochim. Acta* **1985**, *811*, 265. (c) Sutin, N. *Prog. Inorg. Chem.* **1983**, *30*, 411. (d) Newton, M. D.; Sutin, N. *Annu. Rev. Phys. Chem.* **1984**, *35*, 437. (e) Sutin, N. *Acc. Chem. Res.* **1982**, *15*, 275. (f) Marcus, R. A. *Rev. Mod. Phys.* **1993**, *65*, 599. (g) Hush, N. *Coord. Chem. Rev.* **1985**, *64*, 135. (h) Barbara, P. F.; Meyer, T. J.; Ratner, M. A. *J. Phys. Chem.* **1996**, *100*, 13148.

(54) If band **I** were the correct assignment for IT(1), $k_{ET} = 4.0 \times 10^{11}$ s^{-1}, for **4**, which is also too slow to be consistent with the time scale marker. This assignment is also consistent with the energy relationships in Figure 6 if bands **II** and **III** are assigned as the $d\pi \rightarrow d\pi$ transitions.

(55) $r(Os-Cl) = 2.4199(6)$ Å in *cis*-$[Os^{II}(bpy)_2(Cl)(NCCH_3)](PF_6)$[10] and $r(Os-Cl) = 2.332(3)$ Å in *cis*-$[Os^{III}(bpy)_2(Cl)(NCCH_3)](NO_3)_2$.[56]

across the μ-N_2 bridge. The mixing of dπ orbitals between Os^{II} and Os^{III} causes a "blending" of oxidation states. This decreases the change in equilibrium displacement between oxidation states and enhances vibrational overlap between reactant and product vibrational levels low in the potential wells. There can be important contributions from vibrational levels well below the barrier crossing even for low-frequency Os−Cl and Os−N modes. For the $v = 0 \rightarrow v' = 0$ transition between the lowest vibrational levels, the form of the vibrational overlap integral is,

$$e^{-s} \cdot \frac{S^v}{v!} \tag{7}$$

S is related to the reduced mass, M, and change in equilibrium displacement, ΔQ_e, by

$$S = {}^1/_2(M\omega/\hbar)(\Delta Q_e)^2 \tag{8}$$

The Localized-to-Delocalized Transition. One result of this study is to reveal the existence of a series of mixed-valence complexes whose properties include elements of both localized and delocalized behavior. The surrounding solvent orientational polarization is averaged and so are ν(bpy) marker vibrations, suggesting that intramolecular electron transfer is rapid on the time scale for their relaxation from the $v = 1$ vibrational level.[57] On the other hand, the ν(N≡N) vibrational marker and molecular structure reveal residual localization.

The localized-to-delocalized transition is driven by electronic coupling across the bridge. The effect of electronic delocalization on the molecular motions coupled to electron transfer can be described as follows:

(a) In the limit that $2H_{DA} > \lambda$, the electronic delocalization energy exceeds λ. The odd electron is delocalized over both sites, as it is in $[(NH_3)_5Os(N_2)Os(NH_3)_5]^{5+}$.

(b) In **4**, **5**, **7**, and **8**, H_{DA} (Table 5) is a small fraction of λ (Table 5), <5% for IT(1). There is sufficient electronic coupling to "blend" Os^{II} and Os^{III} electronic character (as manifested in decreased Os−Cl and Os−N bond distance changes), but not to cause delocalization.

(c) The discrepancy between ν(N≡N) and orientational motions in the solvent as oxidation state markers is a time scale effect. It is a manifestation of having multiple molecular motions with different time scales coupled to the same process. Intramolecular electron transfer is more rapid than solvent dipole reorganization but slower than the time scale for ν(N≡N).

(d) Molecular vibrations can couple to the change in electronic structure associated with electron transfer in different ways. For the coupled Os−Cl, Os−N modes, there are significant changes in equilibrium displacement, ($S \neq 0$) and they create the barrier to electron transfer. The ν(bpy) vibrations act as "spectator modes" with frequency averaging providing a measure of electron-transfer time scale.[57]

Acknowledgments are made to the National Science Foundation under Grant Numbers CHE-9503738 and CHE-9321413 and to Cavan Fleming for experimental assistance. E-S.E-S. wishes to thank the Egyptian Government for the Data Collection Grant. We also want to thank Prof. Clifford P. Kubiak for sharing information prior to publication.

Supporting Information Available: Table 1 with near-IR data in various solvents, Table 2 with K_{com} values, and Figure 1 with near-IR spectra plotted as $\int \epsilon(\bar{\nu})\, d\bar{\nu}/\bar{\nu}$ (PDF). See any current masthead page for Web access instructions.

JA982802O

(56) Demadis, K. D.; Meyer, T. J.; White, P. S. Unpublished results.

(57) (a) Ito, T.; Hamaguchi, T.; Nagino, H.; Yamaguchi, T.; Washington, J.; Kubiak, C. P. *Science* **1997**, *277*, 660. (b) Kubiak, C. P. Personal communication.